Article

Effect of Gamma-ray Irradiation on the Growth of Au Nano-particles Embedded in the Germano-silicate Glass Cladding of the Silica Glass Fiber and its Surface Plasmon Resonance Response

Seongmin Ju and Won-Taek Han*

School of Electrical Engineering and Computer Science, Gwangju Institute of Science and Technology, Gwangju 61005, South Korea; jusm@gist.ac.kr (S. J.)

* Correspondence: wthan@gist.ac.kr; Tel.: +82-62-715-2215

Abstract: The effect of γ-ray irradiation on surface plasmon resonance (SPR) sensing capability of refractive index (n = 1.418–1.448) of the silica glass optical fiber comprised of germano-silicate glass cladding embedded with Au nano-particles (NPs) was investigated. As the γ-ray irradiation increased from 1 hour to 3 hours with the dose rate of 1,190 Gy/h, the morphology of the Au NPs and the SPR spectrum were found to change. The average diameter of Au NPs increased with the aspect ratio from 1 to 2 and the nano-particles became grown to the clusters. The SPR peak wavelength shifted towards longer wavelength with the increase of total dose of γ-ray irradiation regardless of the corresponding refractive indices. The SPR sensitivities (wavelength/refractive index unit, nm/RIU) also increased from 407 nm/RIU to 3,553 nm/RIU, 1,483 nm/RIU, and 2,335 nm/RIU after the γ-ray irradiation at the total dose of 1,190 Gy, 2,380 Gy, and 3,570 Gy, respectively.

Keywords: γ-ray irradiation; surface plasmon resonance; fiber sensor; nano-particles; cladding embedded optical fiber.

1. Introduction

Transparent host materials embedded with noble metal nano-particles (NPs) such as Au and Ag are of great interest due to its unique characteristics of surface plasmon resonance (SPR) arising from the excitation of electron density oscillations around metal NPs [1–9]. Their SPR property has been widely used in the sensing of chemical, physical, and biological quantities [10–18]. The position and intensity of SPR band depend on the size, shape, and inter-particle separation of the NPs and the dielectric property of the matrix surrounding the NPs [3–4,7,19–27]. The position of SPR peak is known to shift towards long or short wavelength upon the change in NPs size. Therefore various fabrication methods of metal NPs with different geometries such as nano-spheres, nano-shells, nano-tubes, nano-cubes, nano-wires, and etc have been proposed to increase the sensitivity and usability of the SPR sensors [7,19,21–25,27–32]. Furthermore, various post-processing techniques of the irradiation by the pulsed laser, the charged ion, and the γ-ray have been investigated to control NPs with desired size and shape [33–40]. Our group has reported a heat treatment method to control the size of NPs in glass fiber [41–42]. Among such post irradiation processing techniques, the high energy irradiation was proven to control effectively the size, shape, and spacing of the NPs by creating ion tracks resulting from Coulomb explosion and/or thermal spikes accompanying the excitations [43–46]**.** Due to the passage of a swift heavy ion, the particles grow and combine into clusters leading to chemical, physical, and optical changes [47].

Recent advances in the SPR application have led to the realization of the optical fibers incorporated with metal NPs and the fibers coated with metal thin layers [48–56]. In the SPR sensor

based on the optical fiber, evanescent wave is formed by the interface between the surface of the optical fiber and the metal NPs embedded or coated on the surface. The fiber-optic SPR sensor is an alternative to overcome the disadvantages of previous conventional prism based SPR sensor because of its attractive advantages of simple and flexible design, compactness, and remote sensing capability for all-optical applications. Recently, we have reported the fiber-optic refractive index sensor using the novel optical fiber incorporated with Au NPs in the cladding [42,57]. In this paper, hence, we report the effect of γ-ray irradiation on the SPR sensing capability by inducing the morphological change in Au NPs embedded in the fiber.

2. Experiments

2.1. Optical fiber for surface plasmon resonance sensor

The fabrication process of the germano-silicate optical fiber embedded with Au NPs in the cladding and the measurement of its SPR sensing property were described in detail in our previous work [42,57–58]. The Au NPs(cladding)-doped glass fiber coated with low refractive index polymer (SSCP Co., Ltd., Ansan-si, Kyunggi-do, South Korea, FIRON UVF PC-375, n = 1.3820 @ 852 nm) was designed for enabling a light to propagate into the cladding not into the core. Note that the refractive index of the cladding was larger than that of the core and the polymer coating. The refractive index difference between the cladding and the core ($\Delta n_{cladding\text{-}core}$) and that between the cladding and the coating ($\Delta n_{cladding\text{-}coating}$) were 0.0015 and 0.0764, respectively. The cladding width and total diameter of the optical fiber were 2.6 μm and 124.3 μm, respectively. Thus, surface plasmon waves are induced around Au NPs in the cladding of the fiber by a light wave traveling through the cladding.

2.2. Verification of existence and morphology of Au nano-particles

To investigate the effect of γ-ray irradiation on change in morphology of Au NPs and the SPR sensing capability, the fabricated fiber was irradiated by γ-ray from a ^{60}Co radiation source (Nordion Inc., Ottawa, Ontario, Canada, MSD Nordion, pencil type/C-188 sealed) with the dose rate of 1,190 Gy/h for 1 hour to 3 hours at room temperature in air. The γ-ray doses were measured using the alanine pellet dosimeter and estimated by electron paramagnetic resonance analysis with BRUKER's e-scan alanine dosimetry system (Bruker Inc., Billerica, MA, USA). Then the samples of the fibers with and without the γ-ray irradiation prepared by the dual beam focused ion beam (FIB; FEI Co., Hillsboro, OR, USA, Helios NanoLab™ FIB 600) method were examined by transmission electron microscope (TEM; FEI Co., Hillsboro, OR, USA, Technai™ G^2 F30 S-Twin 300 KeV) to confirm the formation and the change in size and distribution of Au NPs. And optical absorption of the fibers was measured to verify again the existence of Au NPs by the cut-back method using the optical spectrum analyzer (OSA; Ando Electric Co., Ltd., Kanagawa Kawasaki-shi, Kanagawa-ken, Japan, AQ 6315B) and white light source (WLS; Ando Electric Co., Ltd., Kawasaki-shi, Kanagawa-ken, Japan AQ 4305).

2.3. Surface palsmon resonance measurement

To characterize SPR sensing property, the change in optical absorption by the irradiation was measured by putting small drops of the refractive index matching oil with various refractive indices (n = 1.418–1.448) on the surface of the stripped portion (3 cm) of the 10 cm fiber (Fig. 1). The coated polymer of the irradiated fiber was stripped off using acetone and then the fiber was spliced with a multi-mode fiber (diameters of core, cladding, coating were 105, 125, and 250 μm, respectively). The light was launched into the multi-mode fiber and the resonance wavelength was measured at the other end of the fiber using the OSA. Note that the change in optical absorption of the fiber without γ-ray irradiation was measured by using the fiber of total length 20 cm [57].

Preprints (www.preprints.org) | NOT PEER-REVIEWED | Posted: 6 March 2019 doi:10.20944/preprints201903.0077.v1

Peer-reviewed version available at Sensors 2019, 19, 1666; doi:10.3390/s19071666

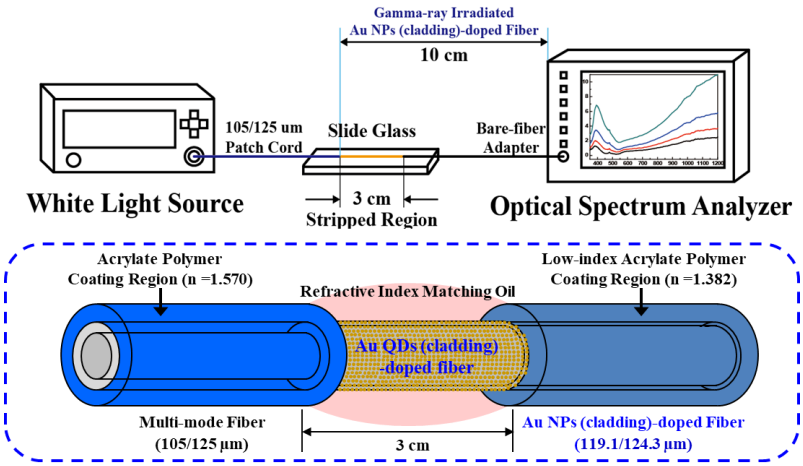

Figure 1. Schematic diagram of the SPR measurement set-up using the optical fiber incorporated with Au NPs in the cladding.

3. Results and Discussion

TEM images and size distributions of Au NPs in the cladding of the fiber before and after the γ-ray irradiation are shown in Fig. 2. The morphology of the Au NPs was dramatically changed with the increase of the γ-ray irradiation dose level from 0 Gy to 1,190 Gy, 2,380 Gy and 3,570 Gy. Before the γ-ray irradiation, the crystalline Au NPs were spherical and uniformly distributed with average diameter of 3.8 nm (2.5 nm–5.2 nm) with the aspect ratio of 1.00. After the irradiation, most of the Au NPs seemed to aggregate and became clusters. As the total dose of the irradiation increased to 1,190 Gy, 2,380 Gy, and 3,570 Gy, the average aspect ratio of the Au NPs increased to 1.05, 1.29, and 2.00, respectively. The size distribution of the Au NPs also increased with the increase of the γ-ray irradiation level. It is clear that the γ-ray irradiation induced the growth of Au NPs by the direct coalescence and consequent transformation from spherical to prolate in shape. The similar growth of crystalline Au NPs in silica glass due to Ostwald ripening by the ion irradiation was also reported [43].

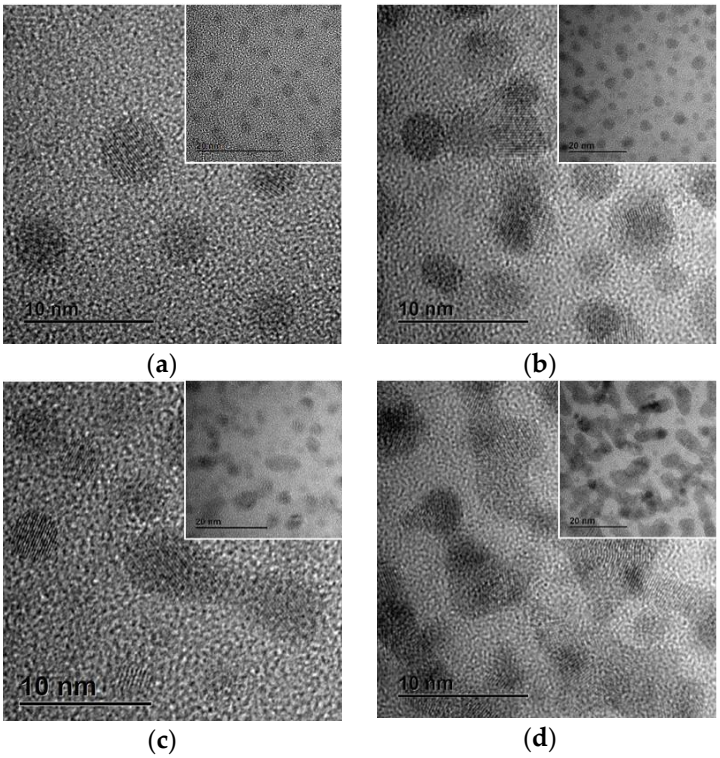

Figure 2. TEM images of the Au NPs incorporated in the cladding of the fiber (a) before and after the γ-ray irradiation at the total dose of (b) 1,190 Gy, (c) 2,380 Gy, and (d) 3,570 Gy.

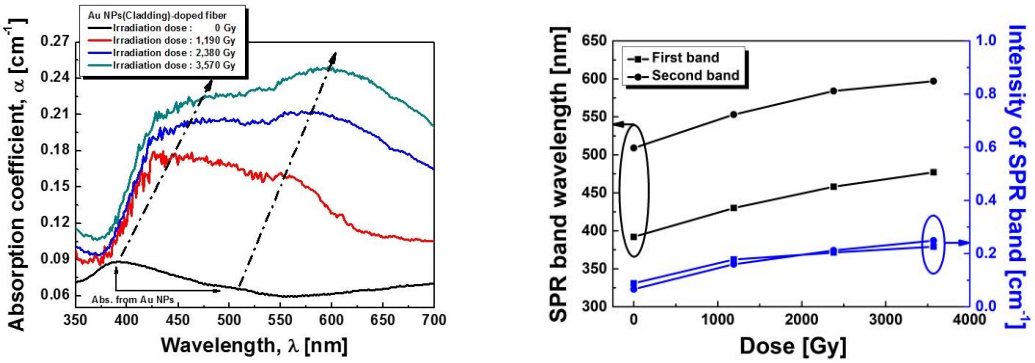

Figure 3. (a) Absorption spectra and (b) peak wavelength and intensity of the SPR band of the optical fiber incorporated with Au NPs before and after the γ-ray irradiation at the total dose of 1,190 Gy, 2,380 Gy, and 3,570 Gy.

To verify the existence of Au NPs in the fiber cladding again, optical absorption was measured by the cut-back method. Fig. 3(a) compares the optical absorption spectra of the fibers before and after the γ-ray irradiation at the total dose of 1,190 Gy, 2,380 Gy, and 3,570 Gy. Before the irradiation, the absorption bands due to SPR were found to appear peaking at 392 nm (absorption coefficient α = 0.088 cm^{-1}) and 509 nm (α = 0.066 cm^{-1}) depending on the particle size and shape of Au NPs in the cladding of the fiber [5,8,42,59]. After the irradiation, the two SPR absorption bands at 392 nm and 509 nm appeared to increase its intensity and to shift towards longer wavelength. The clear appearance of the bands indicates the significant morphological change of the Au NPs as shown in Fig 2. The first SPR absorption band shifted from 392 nm to 430 nm, 458 nm, and 477 nm and the second absorption band from 509 nm to 553 nm, 584 nm, and 597 nm with the increase of the total dose to 1,190 Gy, 2,380 Gy, and 3,570 Gy, respectively. With the increase of γ-ray irradiation dose, the splitting of the SPR absorption bands became more distinct [2,49–51]. It is known that the anisotropically shaped metal particles show a splitted SPR absorption band due to transverse and longitudinal modes of charge density oscillations in the presence of electromagnetic radiation [43]. Thus the splitting of the SPR absorption bands may be due to the morphological change, especially the increase of the aspect ratio, of the Au NPs. As the total dose of γ-ray irradiation increased, the SPR absorption bands wavelength showed a tendency to shift towards longer wavelength due to the growth of Au NPs from spherical to prolate in shape as shown in Fig. 3(b).

Also, the intensity of the two SPR absorption bands increased significantly with the increase of γ-ray irradiation. This absorption increase may be due to the radiation-induced defects. The possible defects are oxygen deficient centers (Si-ODC, ≡Si-Si≡ at 394 nm), per-oxy radicals (Si-POR, ≡Si-O-O· at 630 nm), self-trapped hole defects (Si-STHs at 477 nm, 574 nm, 663 nm, 765 nm), non-bridging oxygen hole centers (Si-NBOHC, ≡Si-O·at 620 nm) due to strained Si-O bonds, GeX (at 475 nm), and Ge-NBOHC (≡Ge-O· at 630 nm) due to strained Ge-O bonds [60–66].

The intensity of the first absorption band corresponding to the Au NPs at the total dose of 1,190 Gy decreased from α = 0.178 cm^{-1} to α = 0.204 cm^{-1} and α = 0.226 cm^{-1} with total dose of 2,380 Gy and 3,570 Gy, respectively. On the other hand, the intensity of the second absorption band corresponding to the Au NP at the total dose of 1,190 Gy increased from α = 0.160 cm^{-1} to α = 0.212 cm^{-1}, and α = 0.249 cm^{-1} at the total dose of 2,380 Gy and 3,570 Gy, respectively. This difference of absorption intensity change depending on the bands is thought to be due to the different morphological behavior of the Au NPs by the γ-ray irradiation.

Preprints (www.preprints.org) | NOT PEER-REVIEWED | Posted: 6 March 2019 doi:10.20944/preprints201903.0077.v1

Peer-reviewed version available at Sensors 2019, 19, 1666; doi:10.3390/s19071666

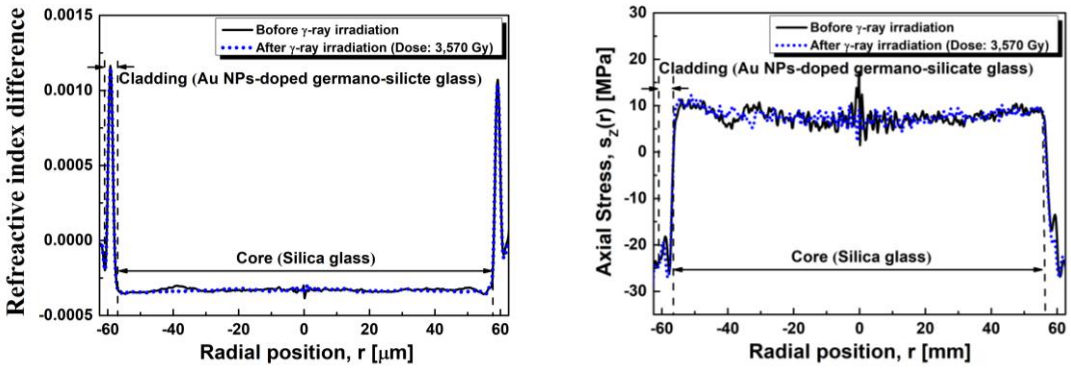

(**a**) (**b**)

Figure 4. (a) Refractive index difference and (b) stress profile of the fiber before and after the γ-ray irradiation with the dose rate of 3,570 Gy.

Considering that the change of the refractive index and the residual stress of the fiber induced by the γ-ray irradiation may affect the transmission characteristics of the optical signal, the refractive index and the residual stress of the fiber before and after the γ-ray irradiation of the total dose of 3,570 Gy were measured by the fiber index profiler (Interfiber Analysis, Sharon, MA, USA, IFA-100) with the accuracy of ± 1 × 10^{-4} and shown in Fig. 4. Before the γ-ray irradiation, the refractive index ($\Delta n_{cladding\text{-}core}$ = 0.0015) of the cladding larger than that of the core was due to the presence of GeO_2 [60,67]. The residual stress of the core was found to be under a tension of 5MPa ~ 10 MPa except the center of the core ~ 17.5 MPa, but that of the cladding was a compression of ~ −26 MPa. The stress in the core is normally positive (tensile) due to the external pulling force during the drawing process. However, the compressive stress in the cladding is developed for the balance of the forces after removing the drawing tension [68–69]. On the other hand, after the γ-ray irradiation at the total dose of 3,570 Gy, no influence on the refractive index was observed. Therefore, the influence of the change in refractive index by the irradiation on SPR characteristics can be excluded. However, a change in the residual stress of the center of the core and the cladding was found. The tensile stress around the center of the core was relaxed from ~ 17.5 MPa to ~ 7.0 MPa without the change of tensile stress of ~ 7.0 MPa in the outer core region. And the compressive stress in the cladding slightly increased from ~ –26 MPa to ~ –27 MPa. Therefore, the negligible change in the refractive index and the residual stress of the cladding by the γ-ray irradiation of the total dose of 3,570 Gy does not contribute to SPR sensing property.

To investigate the effect of the γ-ray irradiation on the SPR sensitivity, the SPR absorption of the Au NPs(cladding)-doped fiber was measured. The SPR absorption was measured by dropping the index matching oils onto the stripped portions of 3 cm. The total fiber length was 10 cm and the refractive index (n = 1.418–1.448) of the matching oils was varied. Figure 5 shows the SPR spectra of the fiber before and after the irradiations of 1,190 Gy, 2,380 Gy, and 3,570 Gy. Before the γ-ray irradiation, two SPR absorption bands were found to appear, the first peak at ~ 380 nm and the second peak at ~ 580 nm [70]. The two SPR absorptions are related to the single Au NPs and the coupled Au NPs, respectively as known from the results shown in Fig. 2 and Fig. 3. The first SPR peak shifted towards longer wavelength from 381.95 nm to 394.15 nm with the increase of the refractive index from 1.418 to 1.448. The intensity of the SPR peak also increased. The SPR sensitivity (wavelength/refractive index unit, nm/RIU) was estimated to be 406.7 nm/RIU. It is well known that the SPR peak wavelength increase with the increase of refractive index is related to the resonance wavelength of the incident light due to the increase of the wave vector of the surface plasmon mode [42,50-52,54,57]. The baseline corrected absorption intensity of the SPR spectrum from 0.80 dB to 4.34 dB increased with the increase of refractive index due to the difference in diffraction orders [52,71]. The full width at half maximum (FWHM) of the SPR band was broadened from 49.06 nm to 71.29 nm with the increase of refractive index due to the spatial spreading and scattering of the conduction electrons [20,42,52,72]. The average SPR absorption intensity and the average FWHM were 2.09 dB

and 60.55 nm, respectively. However, the second SPR band wavelength ~ 580 nm was hard to define its appearance as shown in Fig. 5(a) and the shift of the SPR band with the increase of the refractive index may be due to low concentration of coupled Au NPs.

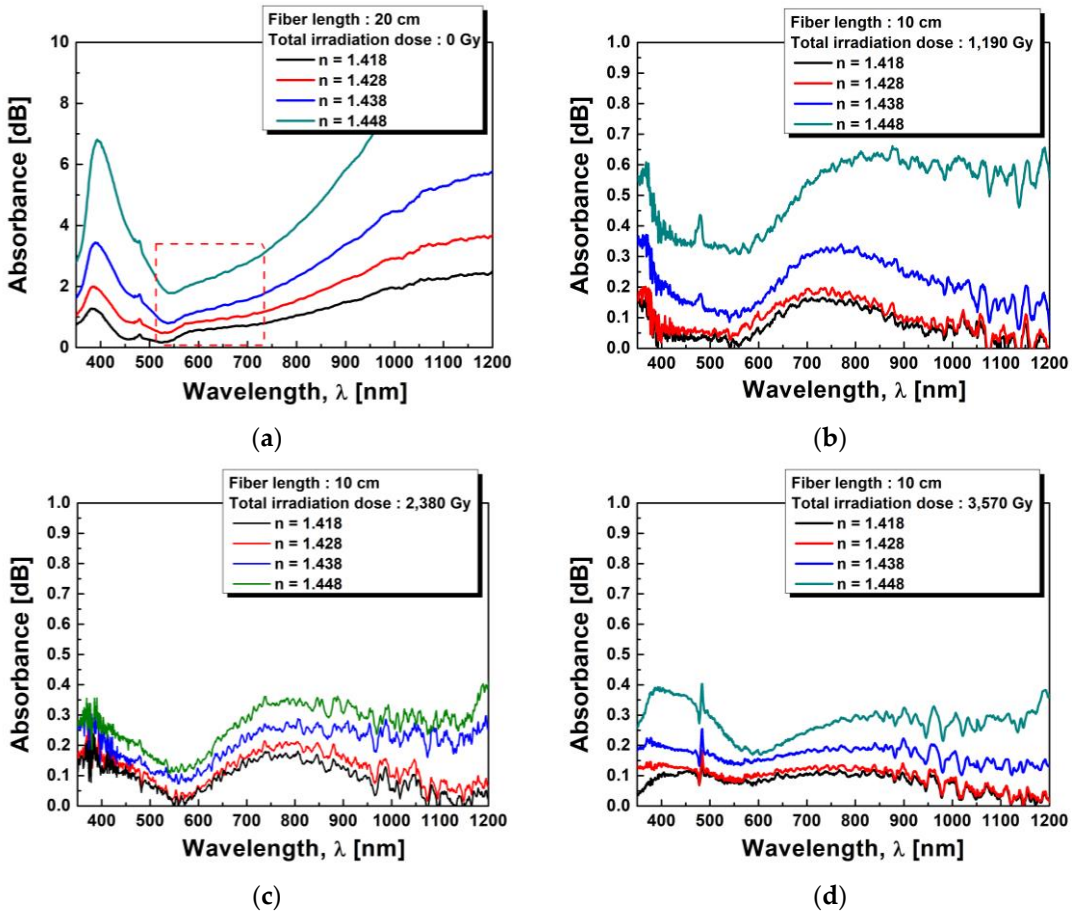

Figure 5. The SPR spectra obtained by dropping the matching oils of different refractive indices (a) before and after the γ-ray irradiation at the total dose of (b)1,190 Gy, (c) 2,380 Gy, and (d) 3,570 Gy.

After the γ-ray irradiation, interestingly, another SPR band was found to appear around 750 nm. This new SPR band may be due to the aggregated Au NPs formed by the γ-ray irradiation as shown in Fig. 2. The intensity of this band increased with the increase of the index. The Au NPs was grown in size and morphologically changed to aggregates due to the bridge-like connection and crosslinking of the Au NPs by the γ-ray irradiation. However, after the γ-ray irradiation of 1,190 Gy, the SPR peak wavelength at 380 nm due to the single Au NPs shifted towards shorter wavelength of 360 nm unexpectedly. And the SPR peak wavelength at 360 nm slightly shifted towards longer wavelength with the increase of the refractive index. The amount of red shift of the SPR band around 750 nm with the increase of the refractive index was much larger than that of the SPR peak at 360 nm and it was due to coupled Au NPs compared to the single Au NPs of the 360 nm peak.

From the results of the SPR spectra as shown in Fig. 5, the variation of the SPR peak wavelength, the SPR sensitivity, the absorption intensity, and the FWHM of the SPR spectrum as a function of refractive index of the matching oils under the γ-ray irradiation were replotted and summarized in Fig. 6. The SPR peak wavelength showed a tendency to shift towards longer wavelength with the increase of the total dose of γ-ray irradiation regardless of the corresponding refractive indices due to the growth and assembly of Au NPs into the Au NP clusters by the γ-ray irradiation (Fig. 6(a)). Also, the onset wavelength of the SPR band around 750 nm was found to shift towards longer wavelength from 527 nm to 559 nm, 572 nm, and 587 nm after the γ-ray irradiation with the increase of the total dose of 1,190 Gy, 2,380 Gy, and 3,570 Gy, respectively. The baseline corrected SPR peak intensity slightly increased from 0.17 dB to 0.24 dB, from 0.17 dB to 0.18 dB, and from 0.07 dB to 0.11

Preprints (www.preprints.org) | NOT PEER-REVIEWED | Posted: 6 March 2019 doi:10.20944/preprints201903.0077.v1

Peer-reviewed version available at Sensors 2019, 19, 1666; doi:10.3390/s19071666

dB with the increase of the refractive index from 1.418 to 1.448 at the total dose of 1,190 Gy, 2,380 Gy, and 3,570 Gy, respectively. The increase of the SPR absorption intensity with the increase of the refractive indices regardless of the γ-ray irradiation is due to leaking out of more divergent light beam from the cladding of the fiber [5,9,73]. However, as the total dose of γ-ray irradiation increased from 1,190 Gy to 3,570 Gy, the SPR absorption intensity decreased regardless of the corresponding refractive indices due to the increase of the radiation-induced loss as shown in Fig. 6(c). And the FWHM of the SPR band became broadened from 230.93 nm to 313.49 nm, from 277.47 nm to 278.52 nm, and from 240.48 nm to 260.96 nm with the increase of the refractive index from 1.418 to 1.448 at the total dose of 1,190 Gy, 2,380 Gy, and 3,570 Gy, respectively. The broadened SPR band with the increase of the refractive indices regardless of the γ-ray irradiation is due to the spatial spreading and scattering of the conduction electrons and the FWHM of the SPR band was saturated with the increase of the total dose of γ-ray irradiation as shown in Fig. 6(d) [20,52,72]. Note that the center wavelength, intensity, and the FWHM of the SPR band were rapidly changed after the γ-ray irradiation at the total dose of 1,190 Gy as compared with the fiber before the γ-ray irradiation. However, the change in center wavelength, intensity, and the FWHM of the SPR band was saturated as the total dose of γ-ray irradiation of 2,380 Gy and 3,570 Gy increased regardless of the corresponding refractive indices.

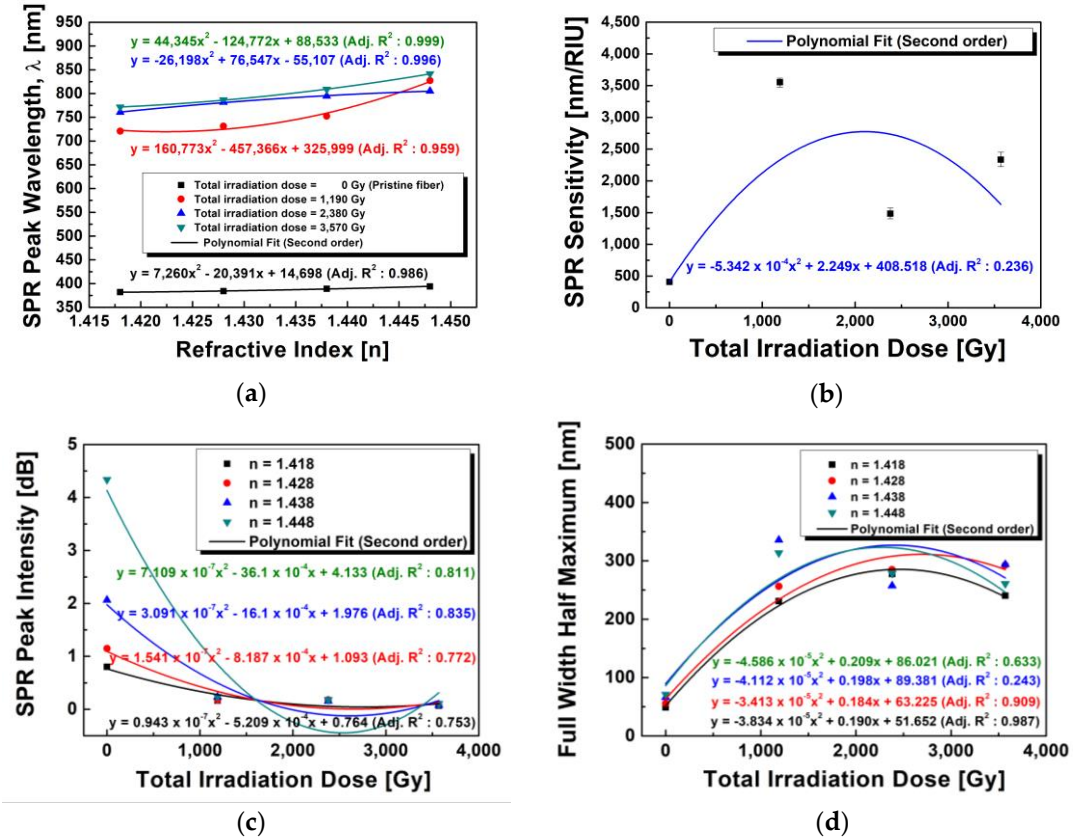

Figure 6. Variation of (a) the SPR peak wavelength, (b) the SPR sensitivity, (c) the absorption intensity, and (d) the FWHM of the SPR spectrum as a function of refractive index of the matching oils before and after the γ-ray irradiation at the total dose of 1,190 Gy, 2,380 Gy, and 3,570 Gy (The lines were polynomial-fitted).

From the results of the SPR spectra as shown in Fig. 6(a), the center wavelengths of the SPR band were found at 720.67 nm, 731.33 nm, 752.29 nm, and 827.27 nm with the increase of the refractive index 1.418, 1.428, 1.438, and 1.448 under at dose of 1,190 Gy, respectively. And under the total dose of 2,380 Gy and 3,570 Gy, the SPR band wavelengths were found to appear at 760.75 nm, 781.71 nm, 794.77 nm, and 805.25 nm and at 771.53 nm, 786.70 nm, 808.65 nm, and 841.57 nm with the increase of the refractive index, respectively. The estimated sensitivities (wavelength/RIU) of the SPR sensor based on the γ-ray irradiated fibers on sensing capability of refractive index (n = 1.418–

1.448) increased to be 407 nm/RIU, 3,553 nm/RIU, 1,483 nm/RIU, and 2,335 nm/RIU before and after the γ-ray irradiation at the total dose of 1,190 Gy, 2,380 Gy, and 3,570 Gy, respectively, as shown in Fig. 6(b). After the γ-ray irradiation, the SPR sensitivity increased rapidly but saturated with the increase of the total dose of γ-ray irradiation. The SPR sensitivity, the average absorption intensity, and the average FWHM of the fiber before and after the γ-ray irradiation at the total dose of 1,190 Gy, 2,380 Gy, and 3,570 Gy are listed in Table. 1. The average SPR absorption intensity and the average FWHM were changed from 0.20 dB to 0.17 dB and 0.08 dB and from 284.21 nm to 274.59 nm and 272.03 nm at the total dose of 1,190 Gy, 2,380 Gy, and 3,570 Gy, respectively. The average absorption intensity and average FWHM of the SPR band around 750 nm in the range of the refractive index from 1.418 to 1.448 decreased with the increase of the total dose of γ-ray irradiation at 1,190 Gy, 2,380 Gy, and 3,570 Gy.

Table 1. The SPR sensitivity, the average absorption intensity, and the average FWHM of the optical fiber embedded with Au NPs in cladding after the γ-ray irradiation.

γ-ray irradiation	Total γ-ray irradiation dose [Gy]	Sensitivity [nm/RIU]	Average absorption intensity [dB]	Average FWHM [nm]
Before	0	407	2.087	60.554
After	1,190	3,553	0.204	284.207
	2,380	1,483	0.170	274.592
	3,570	2,335	0.084	272.026

From the SPR results of the fibers after the γ-ray irradiation, the growth of the Au NPs to anisotropically shaped Au cluster must have played an important role because it showed the splitting of the SPR band into the transverse and longitudinal modes [43]. The increase in the aspect ratio of the Au cluster led to red shifts of the longitudinal SPR band (longer wavelength) and it showed better sensitivity in response to changes in refractive index of the surrounding medium because the refractive index sensitivity of the SPR sensor was enhanced with increasing SPR band wavelength [74]. However, an excessive γ-ray irradiation is detrimental due to the decrease of the SPR sensitivity and the increase of the radiation-induced optical loss by excessively changing the size and shape of Au NPs. Nevertheless, the γ-ray irradiation of the SPR sensor fiber with an appropriate irradiation dose is an effective method to increase the SPR sensitivity and to control a desired detection wavelength for utilizing commercially available light source and power detector.

4. Conclusions

The silica glass optical fiber incorporated with Au NPs in the germano-silicate glass cladding has been irradiated by ^{60}Co γ-rays with the dose rate of 1,190 Gy/h for 1 hour to 3 hours at room temperature to investigate the enhancement of the SPR sensitivity and the enabling tunability of operation range of sensing wavelength of the SPR for the refractive index sensing by controlling the size and shape of the incorporated crystalline Au NPs in the fiber cladding. As the total dose of the γ-ray irradiation increased to 1,190 Gy, 2,380 Gy and 3,570 Gy, the average aspect ratio of the Au NPs increased from 1.0 to 1.05, 1.29, and 2.00, respectively together with the increase of the particles size. The spherical Au NPs of ~ 3.8 nm diameter grew into the large clusters by the direct coalescence of NPs and then transformed to prolate shaped particles with large aspect ratio.

The SPR absorption was also related with the Au NPs and thus the shift and bimodal appearance of the SPR bands implies that Au NPs was grown in size with the morphologically change by the γ-ray irradiation. After the irradiation, the two SPR absorption bands at 392 nm and 509 nm appeared to increase its intensity and to shift towards longer wavelength. Also, with the increase of γ-ray irradiation dose, the splitting of the SPR absorption bands became more distinct due to the increase of the aspect ratio of the Au NP clusters.

No significant change in the refractive index and the residual stress after the γ-ray irradiation at the total dose of 3,570 Gy indicated no contribution of them to the SPR sensing capacity. With the increase of the refractive index from 1.418 to 1.448, the SPR peak shifted towards longer wavelength. Furthermore, the major SPR band peaking at 380 nm was found to change around 750 nm after the γ-ray irradiation for the corresponding refractive indices (n = 1.418–1.448), increased with the increase of the index, respectively. The SPR sensitivity of the fiber increased rapidly but saturated from 406.7 nm/RIU to 3,553 nm/RIU, 1,483 nm/RIU, and 2,335 nm/RIU with the increase of the total dose of γ-ray irradiation from 0 Gy to 1,190 Gy, 2,380 Gy, and 3,570 Gy, respectively. However, the average SPR absorption intensity decreased from 0.20 dB to 0.17 dB and 0.08 dB and the average FWHM of the SPR band around 750 nm also decreased from 284.21 nm to 274.59 nm and 272.03 nm with the increase of the total dose of γ-ray irradiation from 1,190 Gy to 2,380 Gy and 3,570 Gy, respectively.

Acknowledgments: This work was supported by the Advanced Technology Radiation Laboratory of the Korea Atomic Energy Research Institute, South Korea.

Funding: This research was partially funded by the KEPCO Research Institute of South Korea under the grant number KEPRI-16-23.

Author Contributions: S. Ju conceived of the study, participated in the design of the experiments, performed the analysis, and wrote the paper; W.-T. Han conceived of the study and coordination and helped to draft the manuscript.

Conflicts of Interest: The authors declare no conflict of interest.

References

1. Homola, J.; Yee, S. S.; Gauglitz, G. Surface plasmon resonance sensors: review. *Sens. Actuators B* 1999, *54*, pp. 3–15.
2. Yonzon, C. R.; Jeoung, E.; Zou, S.; Schatz, G. C.; Mrksich, M.; Duyne, R. P. V. A comparative analysis of localized and propagating surface plasmon resonance sensors: The binding of concanavalin A to a monosaccharide functionalized self-assembled monolayer. *J. Am. Chem. Soc.* 2004, *126*, pp. 12669–12676.
3. Nath, N.; Chilkoti, A. Label-free biosensing by surface plasmon resonance of nanoparticles on glass: optimization of nanoparticle size. *Anal. Chem.* 2004, *76*, pp. 5370–5378.
4. Yu, F.; Ahl, S.; Caminade, A.-M.; Majoral, J.-P.; Knoll, W.; Erlebacher, J. Simultaneous excitation of propagating and localized surface plasmon resonance in nanoporous gold membranes. *Anal. Chem.* 2006, *78*, pp. 7346–7350.
5. Garcia, M. A. Corrigendum: Surface plasmons in metallic nanoparticles: fundamentals and applications. *J. Phys. D: Appl. Phys.* 2012, *45*, pp. 389501–1–20.
6. Peng, T.-C.; Lin, W.-C.; Chen, C.-W.; Tsai, D. P.; Chiang, H.-P. Enhanced sensitivity of surface plasmon resonance phase-interrogation biosensor by using silver nanoparticles. *Plasmonics* 2011, *6*, pp. 29–34.
7. Lee, K.-S.; El-Sayed, M. A. Gold and silver nanoparticles in sensing and imaging: sensitivity of plasmon response to size, shape, and metal composition. *J. Phys. Chem. B* 2006, *110*, pp. 19220–19225.
8. Sönnichsen, C.; M.Reinhard, B.; Liphardt, J.; Alivisatos, A. P. A molecular ruler based on plasmon coupling of single gold and silver nanoparticles. *Nature Biotechnol.* 2005, *23*, pp. 741–745.
9. Luther, J. M.; Jain, P. K.; Ewers, T.; Alivisatos, A. P. Localized surface plasmon resonances arising from free carriers in doped quantum dots. *Nature Mater.* 2011, *10*, pp. 361–366.
10. Singh, S.; Gupta, B. D. Simulation of a surface plasmon resonance-based fiber-optic sensor for gas sensing in visible range using films of nanocomposites. *Meas. Sci. Technol.* 2010, *21*, pp. 115202–1–8.
11. Jorgenson, R. C.; Yee, S. S. A fiber-optic chemical sensor based on surface plasmon resonance. *Sens. and Actuators B: Chem.* 1993, *12*, pp. 213–220.
12. Matsubara, K.; Kawata, S.; Minami, S. Optical chemical sensor based on surface plasmon measurement. *Appl. Opt.* 1998, *27*, pp. 1160–1163.
13. Liedberg, B.; Nylander, C.; Lunström, I. Surface plasmon resonance for gas detection and biosensing. *Sens. Actuators* 1983, *4*, pp. 299–304.
14. Sharma, S. K.; Gupta, B. D. Simulation of a localized surface-plasmon-resonance-based fiber optic temperature sensor. *Opt. Soc. Am. A* 2010, *27*, pp. 1743–1749.

15. Homola, J. Present and future of surface plasmon resonance biosensors. *Anal. Bioanal. Chem.* 2003, *377*, pp. 528–539.
16. Haes, A. J.; Hall, W. P.; Chang, L.; Klein, W. L.; Van Duyne, R. P. A localized surface plasmon resonance biosensor: first steps toward an assay for Alzheimer's disease. *NANO Letter* 2004, *4*, pp. 1029–1034.
17. Lin, Y.; Zou, Y.; Lindquist, R. G. A reflection-based localized surface plasmon resonance fiber-optic probe for biochemical sensing. Biomed. *Opt. Express* 2011, *2*, pp. 478–484.
18. Anker, J. N.; Hall, W. P.; Lyandres, O.; Shan, N. C.; Zhao, J.; Duyne, R. P. V. Biosensing with plasmonic nanosensors. *Nature Mater.* 2008, *7*, pp. 442–453.
19. Chung, P.-Y.; Lin, T.-H; Schultz, G.; Batich, C.; Jiang, P. Nanopyramid surface plasmon resonance sensors. *Appl. Phys. Lett.* 2010, *96*, pp. 261108–1–3.
20. Zhang, Y.; Yuwono, A. H.; Li, J.; Wang, J. Highly dispersed gold nanoparticles assembled in mesoporous titania films of cubic configuration. *Micropor. Mesopor. Mater.* 2008, *110*, pp. 242–249.
21. Jensen, T. R.; Schatz, G. C.; Van Duyne, R. P. Nanosphere lithography: Surface plasmon resonance spectrum of a periodic array of silver nanoparticles by ultraviolet-visible extinction spectroscopy and electrodynamic modeling. *J. Phys. Chem. B* 1999, *103*, pp. 2394–2401.
22. Chang, S. H.; Gray, S. K.; Schatz, G. C. Surface plasmon generation and light transmission by isolated nanoholes and arrays of nanoholes in thin metal films. *Opt. Express* 2005, *13*, pp. 3150–3165.
23. Aizpurua, J.; Hanarp, P.; Sutherland, D. S.; Kall, M.; Bryant, G. W.; de Abajo, F. J. G. Optical properties of gold nanorings. *Phys. Rev. Lett.* 2003, *90*, pp. 057401–1–4.
24. Fu, J.; Park, B.; Zhao, Y. Nanorod-mediated surface plasmon resonance sensor based on effective medium theory. *App. Opt.* 2009, *48*, pp. 4637–4649.
25. Kim, J.; Liu, G. L.; Lu, Y.; Lee, L. P. Spectral tuning of localised surface plasmon-polariton resonance in metallic nano-crescents. *IEE Proc.-Nanobiotechnol.* 2006, *153*, pp. 42–46.
26. Liu, Z. W.; Wei, Q. H.; Zhang, X. Surface plasmon interference nanolithography. *Nano. Lett.* 2005, *5*, pp. 957–961.
27. Halas, N. Playing with plasmons: tuning the optical resonant properties of metallic nanoshells. *MRS Bull.* 2005, *30*, pp. 362–367.
28. Takahata, R.; Yamazoe, S.; Koyasu, K.; Tsukuda, T. Surface plasmon resonance in gold ultrathin nanorods and nanowires. *J. Am. Chem. Soc.* 2014, *136*, pp. 8489–8491.
29. Zhang, Q.; Hu, Y.; Guo, S.; Goebl, J.; Yin, Y. Seeded growth of uniform Ag nanoplates with high aspect ratio and widely tunable surface plasmon bands. *Nano Lett.* 2010, *10*, pp. 5037–5042.
30. Zhu, J.; Deng, X.-C. Improve the refractive index sensitivity of gold nanotube by reducing the restoring force of localized surface plasmon resonance. *Sens. Actuators B: Chem.* 2011, *155*, pp. 843–847.
31. Mahmoud, M. A.; El-Sayed, M. A. Time dependence and signs of the shift of the surface plasmon resonance frequency in nanocages elucidate the nanocatalysis mechanism in hollow nanoparticles. *Nano Lett.* 2011, *11*, pp. 946–953.
32. Ringe, E.; McMahon, J. M.; Sohn, K.; Cobley, C.; Xia, Y.; Huang, J.; Schatz, G. C.; Marks, L. D.; Van Duyne, R. P. Unraveling the effects of size, composition, and substrate on the localized surface plasmon resonance frequencies of gold and silver nanocubes: A systematic single-particle approach. *J. Phys. Chem. C*, 2010, *114*, pp. 12511–12516.
33. Mallick, K.; Wang, Z. L.; Pal, T. Seed-mediated successive growth of gold particles accomplished by UV irradiation: a photochemical approach for size-controlled synthesis. *J. Photochem. Photobiol. A: Chem.* 2001, *140*, pp. 75–80.
34. Stamplecoskie, K. G.; Scaiano, J. C. Light emitting diode irradiation can control the morphology and optical properties of silver nanoparticles. *J. Am. Chem. Soc.* 2010, *132*, pp. 1825–1827.
35. Stellacci, F.; Bauer, C. A.; Meyer-Friedrichsen, T.; Wenseleers, W.; Alain, V.; Kuebler, S. M.; Pond, S. J. K.; Zhang, Y.; Marder, S. R.; Perry, J. W. Laser and electron-beam induced growth of nanoparticles for 2D and 3D metal patterning. *Adv. Mater.* 2002, *14*, pp. 194–198.
36. Abid, J. P.; Wark, A. W.; Brevet, P. F.; Girault, H. H. Preparation of silver nanoparticles in solution from a silver salt by laser irradiation. *Chem. Commun.* 2002, *7*, pp. 792–793.
37. Mishra, Y. K.; Avasthi, D. K.; Kulriya, P.K.; Singh, F.; Kabiraj, D.; Tripathi, A.; Pivin, J. C.; Bayer, I. S.; Biswas, A. Controlled growth of gold nanoparticles induced by ion irradiation: An in situ x-ray diffraction study. *Appl. Phys. Lett.* 2007, *91*, pp. 073110–1–3.
38. Valentin, E.; Bernas, H.; Ricolleau, C.; Creuzet, F. Ion Beam "Photography": Decoupling nucleation and growth of metal clusters in glass. *Phys. Rev. Lett.* 2001, *86*, pp. 99–102.

39. Chen, P.; Song, L.; Liu, Y.; Fang, Y. Synthesis of silver nanoparticles by γ-ray irradiation in acetic water solution containing chitosan. *Radiat. Phys. Chem.* 2007, *76*, pp. 1165–1168.
40. Yokan, R.; Chirachanchai, S. Silver nanoparticles dispersing in chitosan solution: Preparation by γ-ray irradiation and their antimicrobial activities. *Mater. Chem. Phys.* 2009, *115*, pp. 296–302.
41. Ju, S.; Watekar, P. R.; Kim, C.; Han, W.-T. Particle size control of PbTe quantum dots incorporated in the germano-silicate glass optical fiber by heat treatment. *J. Non-Cryst. Solids* 2010, *356*, pp. 2273–2276.
42. Ju, S.; Jeong, S.; Kim, Y.; Lee, S.-H.; Linganna, K.; Kim, C. J.; Han, W.-T. Effect of heat treatment of optical fiber incorporated with Au nano-particles on surface plasmon resonance. *Opt. Mater. Express* 2015, *5*, pp. 1440–1449.
43. Mishra, Y. K.; Singh, F.; Pivin, J. C.; Malinovska, D.; Pippel, E.; Avasthi, D. K. Synthesis of elongated Au nanoparticles in silica matrix by ion irradiation. *Appl. Phys. Lett.* 2007, *91*, pp. 063103–1–3.
44. D'Orléans, C.; Stoquert, J. P.; Estournès, C.; Cerruti, C.; Grob, J. J.; Guille, J. L.; Haas, F.; Muller, D.; Richard-Plouet, M. Anisotropy of Co nanoparticles induced by swift heavy ions. *Phys. Rev. B* 2003, *67*, pp. 220101–1–4.
45. Daniel, M.-C.; Astruc, D. Gold nanoparticles: Assembly, supramolecular chemistry, quantum-size-related properties, and applications toward biology, catalysis, and nanotechnology. *Chem. Rev.* 2004, *104*, pp. 93–346.
46. Bringa, E. M.; Johnson, R. E. Coulomb explosion and thermal spikes. *Phys. Rev. Lett.* 2002, *88*, pp. 165501–1–4.
47. Joseph, B.; Ghatak, J.; Lenka, H. P.; Kuiri, P. K.; Sahu, G.; Mishra, N. C.; Mahapatra, D. P. Effect of 100 MeV Au irradiation on embedded Au nanoclusters in silica glass. *Nucl. Instr. and Meth. in Phys. Res. B* 2007, *256*, pp. 659–664.
48. Slavík, R.; Homola, J.; Čtyroký, J.; Brynda, E. Novel spectral fiber optic sensor based on surface plasmon resonance. *Sens. Actuators B: Chem.* 2001, *74*, pp. 106–111.
49. Sharma, A. K.; Jha, R.; Gupta, B. D. Fiber-optic sensors based on surface plasmon resonance: A comprehensive review. *IEEE Sens. J.* 2007, *7*, pp. 1118–1129.
50. Gupta, B. D.; Verma, R. K. Surface plasmon resonance-based fiber optic sensors: Principle, probe designs, and some applications. *J. Sens.* 2009, *2009*, pp. 1–12.
51. Mitsushio, M.; Higashi, S.; Higo, M. Construction and evaluation of a gold-deposited optical fiber sensor system for measurements of refractive indices of alcohols. *Sens. Actuators A: Phys.* 2004, *111*, pp. 252–259.
52. Ju, S.; Jeong, S.; Kim, Y.; Jeon, P.; Park, M.-S.; Jeong, H.; Boo, S.; Jang, J.-H.; Han, W.-T. Experimental demonstration of surface plasmon resonance enhancement of the tapered optical fiber coated with Au/Ti thin film. *J. Non-Cryst. Solids* 2013, *383*, pp. 146–152.
53. Singh, S.; Verma, R. K.; Gupta, B. D. Surface plasmon resonance based fiber optic sensor with symmetric and asymmetric metallic coatings: a comparative study. *Sensors and Transducers J.* 2009, *100*, pp. 116–124.
54. Jeong, H.-H.; Erdene, N.; Park, J.-H.; Jeong, D.-H.; Lee, S.-K. Analysis of fiber-optic localized surface plasmon resonance sensor by controlling formation of gold nanoparticles and its bio-application. *J. Nanosci. Nanotechno.* 2012, *12*, pp. 7815–7821.
55. Lee, B.; Roh, S.; Park, J. Current status of micro- and nano-structured optical fiber sensors. *Opt. Fiber Technol.* 2009, *15*, pp. 209–221.
56. Shevchenko, Y. Y.; Albert, J. Plasmon resonances in gold-coated tilted fiber Bragg grating. *Opt. Lett.* 2007, *32*, pp. 211–213.
57. Ju, S.; Jeong, S.; Kim, Y.; Lee, S.-H.; Han, W.-T. Surface plasmon resonance characteristics of optical fiber incorporated with Au nano-particles in cladding region. *J. Nanosci. Nanotechnol.* 2016, *16*, pp. 6308–6312.
58. Ju, S.; Jeong, S.; Kim, Y.; Jeon, P.; Boo, S.; Han, W.-T. Development of specialty optical fiber incorporated with Au nano-particles in cladding for surface plasmon resonance sensors. *Sensors and Transducers J.* 2013, *18*, pp. 76–83.
59. Roman, J. E.; Wincik, K. A. Photowritten gratings in ion-exchanged glass waveguides. *Opt. Lett.* 1993, *18*, pp. 808–810.
60. Girard, S.; Kuhnhenn, J.; Gusarov, A.; Brichard, B.; Van Uffelen, M.; Ouerdane, Y.; Boukenter, A.; Marcandella, C. Radiation effects on silica-based optical fibers: Recent advances and future challenges. *IEEE Trans. Nucl. Sci.* 2013, *60*, pp. 2015–2036.
61. Kim, Y.; Ju, S.; Jeong, S.; Lee, S. H.; Han, W.-T. Gamma-ray radiation response at 1550 nm of fluorine-doped radiation hard single-mode optical fiber. *Opt. Express* 2016, *24*, pp. 3910–3920.

62. Regnier, E.; Flammer, I.; Girard, S.; Gooijer, F.; Achten, F.; Kuyt, G. Low-dose radiation-induced attenuation at infrared wavelengths for P-doped, Ge-doped and pure silica-core optical fibres. *IEEE Trans. Nucl. Sci.* 2007, *54*, pp. 1115–1119.
63. Origlio, G.; Boukenter, A.; Girard, S.; Richard, N.; Cannas, M.; Boscaino, R.; Ouerdane, Y. Irradiation induced defects in fluorine doped silica. *Nucl. Instrum. Methods Phys. Res. Sect. B* 2008, *266*, pp. 2918–2922.
64. Kajihara, K.; Hirano, M.; Skuja, L.; Hosono, H. ^{60}Co γ-ray-induced intrinsic defect processes in fluorine-doped synthetic SiO_2 glasses of different fluorine concentrations. *Mater. Sci. Eng. B* 2009, *161*, pp. 96–99.
65. Giacomazzi, L.; Martin-Samos, L.; Boukenter, A.; Ouerdane, Y.; Girard, S.; Richard, N. Ge(2), Ge(1) and Ge-E′ centers in irradiated Ge-doped silica: a first-principles EPR study. *Opt. Mater. Express* 2015, *5*, pp. 1054–1064.
66. Kyoto, M.; Chigusa, Y.; OOE, M.; Watanabe, M.; Matubara, T.; Yamamoto, T.; Okamoto, S. Gamma-ray irradiation effect on loss increase of single mode optical fibers, (I). *J. Nucl. Sci. Technol.* 1989, *26*, pp. 507–515.
67. Chu, P. L.; Whitbread, T. Measurement of stresses in optical fiber and preform. *Appl. Opt.* 1982, *21*, pp. 4241–4245.
68. Kim, B. H.; Park, Y.; Ahn, T.-J.; Kim, D. Y.; Lee, B. H.; Chung, Y.; Paek, U.-C.; Han, W.-T. Residual stress relaxation in the core of optical fiber by CO_2 laser irradiation. *Opt. Lett.* 2001, *26*, pp. 1657–1659.
69. Kim, B. H.; Ahn, T.-J.; Kim, D. Y.; Lee, B. H.; Chung, Y.; Paek, U.-C.; Han, W.-T. Effect of CO_2 laser irradiation on the refractive-index change in optical fibers. *Appl. Opt.* 2002, *41*, pp. 3809–3815.
70. Chen, H.; Kou, X.; Yang, Z.; Ni, W.; Wang, J. Shape- and size-dependent refractive index sensitivity of gold nanoparticles. *Langmuir* 2008, *24*, pp. 5233-5237.
71. Dou, X.; Phillips, B. M.; Chung, P.-Y.; Jiang, P. High surface plasmon resonance sensitivity enabled by optical disks. *Opt. Lett.* 2012, *37*, pp. 3681–3683.
72. Lee, M.; Chae, L.; Lee, K. C. Microstructure and surface plasmon absorption of sol-gel-prepared Au nanoclusters in TiO_2 thin films. *NanoStruct. Mater.* 1999, *11*, pp. 195–201.
73. Yeri, A. S.; Gao, L.; Gao, D. Mutation screening based on the mechanical properties of DNA molecules tethered to a solid surface. *J. Phys. Chem. B* 2010, *114*, pp. 1064–1068.
74. Kazuma, E.; Tatsuma, T. Localized surface plasmon resonance sensors based on wavelength-tunable spectral dips. *Nanoscale* 2014, *6*, pp. 2397–2405.